

# High harmonic generation in fullerene molecules

H. K. Avetissian,<sup>1</sup> A. G. Ghazaryan,<sup>1</sup> and G. F. Mkrtchian<sup>1,\*</sup>

<sup>1</sup>*Centre of Strong Fields Physics, Yerevan State University, 0025, Yerevan, Armenia*

(Dated: August 13, 2021)

Using dynamical Hartree-Fock mean-field theory, we study the high-harmonic generation (HHG) in the fullerene molecules  $C_{60}$  and  $C_{70}$  under strong pump wave driving. We consider a strong-field regime and show that the output harmonic radiation exhibits multiple plateaus, whose borders are defined by the molecular excitonic lines and cutoff energies within each plateau scale linearly with the field strength amplitude. In contrast to atomic cases for the fullerene molecule, with the increase of the pump wave photon energy the cutoff harmonic energy is increased. We also show that with the increase of the electron-electron interaction energy overall the HHG rate is suppressed. We demonstrate that the  $C_{70}$  molecule shows richer HHG spectra and a stronger high-harmonic intensity than the  $C_{60}$ .

**Introduction**— An intense light interaction with a quantum system can excite the system's electrons towards extreme nonequilibrium states during a fraction of its cycle [1, 2]. Excited by the wavefield and subjected to the internal forces inside the system, the electrons emit coherent electromagnetic (EM) radiation that can contain from tens to many hundreds of harmonics of an incident light [3, 4]. This is one of the fundamental processes in the intense laser-matter interaction called high harmonic generation (HHG) [5]. The HHG process in atoms or molecules with the three-step model [6] explanation is a well-demonstrated method for producing coherent extreme ultraviolet radiation. The coherent spectrum of HHG implies access to the extreme time resolution of the underlying quantum dynamics that opens the way for attosecond physics [7, 8] and ultrafast imaging methods for emitters themselves. In particular, using HHG spectroscopy one can reconstruct the crystal potential [9], observe Mott [10] and Peierls [11] transitions, retrieve the band structure [12, 13].

For HHG it is crucial to increase HHG conversion efficiency and to extend the harmonics cutoff [14]. Specifically, the conversion efficiency of the HHG process strongly depends on the density of emitters and the density of states of emitters. The use of molecular systems, clusters, and crystals can significantly increase the harmonic intensity by utilizing multiple excitation channels [15–17]. Thus, in the last decade, there has been a growing interest to extend HHG to crystals [18–26] and two-dimensional nanostructures, such as semimetallic graphene [27–38], semiconductor transition metal dichalcogenides [39, 40], and dielectric hexagonal boron nitride [41]. Currently, this is a new growing research field – extreme nonlinear optics of nanostructured materials.

Among the variety of nanostructured materials, carbon allotropes play a central role. The discovery of fullerene  $C_{60}$  [42] through laser evaporation of graphite and its synthesis in macroscopic amounts [43] was triggered the study of many other carbon nanostructures, such as carbon nanotubes [44], graphene and its derivatives [45]. Currently, carbon nanomaterials are promising materials for many applications, and in particular for extreme nonlinear optics. Being the member of the carbon allotropes, it is expected a strong HHG from fullerene molecules. Experimentally, in Refs. [46, 47] it is reported a strong harmonic signal from  $C_{60}$  plasma. Theoretical

works predicted a strong HHG from a  $C_{60}$  molecule [48–50] and solid  $C_{60}$  [51]. The theoretical analyses in Refs. [48–50] are dominated by a single-particle picture, but it is unclear how the electron-electron Coulomb interaction leaves its mark on HHG and sub-cycle electronic response in these materials. Besides, in [48], moderately strong fields were considered, and excitonic lines were termed as noninteger harmonics. However, these intrinsic exciton lines are the result of Raman scattering of light, not harmonic radiation. Another problem is how the symmetry groups of the most abundant fullerenes  $C_{60}$  and  $C_{70}$ , namely the icosahedron group and the dihedral group, affect the HHG process in these materials.

In the present work, we develop a microscopic theory of a fullerene molecule nonlinear interaction with strong EM radiation of linear polarization taking into account electron-electron interaction (EEI). In particular, we consider  $C_{60}$  and  $C_{70}$  molecules as the most abundant examples of fullerene molecules with different point group symmetries. By means of the dynamical Hartree-Fock approximation, we reveal the general and basal structure of the HHG spectrum and its relation to the molecular excitations.

**Model**— Let a fullerene molecule,  $C_{60}$  or  $C_{70}$ , interact with strong coherent EM radiation that results in HHG. We assume neutral fullerene molecules, which will be described in the scope of the tight-binding theory where the interball hopping is much smaller than the on-ball hopping, and EEI is described in the extended Hubbard approximation [52–55]. Hence, the total Hamiltonian reads:

$$\hat{H} = \hat{H}_0 + \hat{H}_{\text{int}}, \quad (1)$$

where

$$\hat{H}_0 = - \sum_{\langle i,j \rangle \sigma} t_{ij} c_{i\sigma}^\dagger c_{j\sigma} + \frac{U}{2} \sum_{i\sigma} n_{i\sigma} n_{i\bar{\sigma}} + \frac{1}{2} \sum_{\langle i,j \rangle} V_{ij} n_i n_j \quad (2)$$

is the free fullerene Hamiltonian. Here  $c_{i\sigma}^\dagger$  creates an electron with the spin polarization  $\sigma = \{\uparrow, \downarrow\}$  at site  $i$  ( $\bar{\sigma}$  is the opposite to  $\sigma$  spin polarization), and  $\langle i, j \rangle$  runs over all the first nearest-neighbor hopping sites with the transfer energy  $t_{ij}$ . The density operator is:  $n_{i\sigma} = c_{i\sigma}^\dagger c_{i\sigma}$ , and the total electron density for site  $i$  is:  $n_i = n_{i\uparrow} + n_{i\downarrow}$ . The second and third terms in (2) describe the

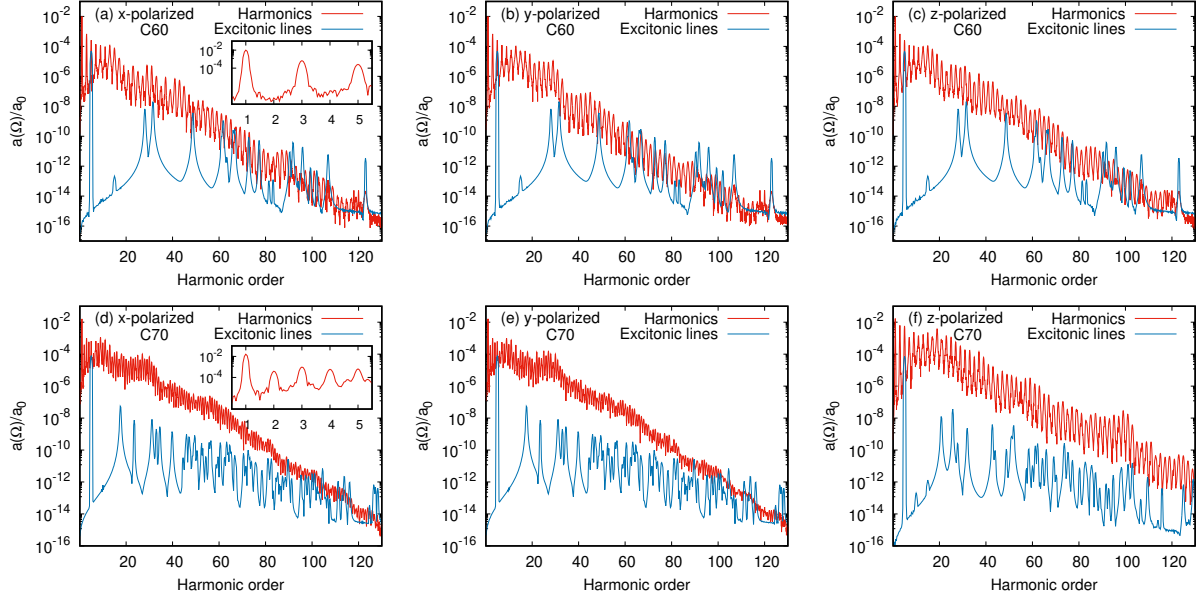


FIG. 1: The HHG spectra in the strong-field regime in logarithmic scale via the normalized dipole acceleration Fourier transformation  $a(\Omega)/a_0$  (in arbitrary units) for  $C_{60}$  (a, b, c) and for  $C_{70}$  (d, e, f). The wave is assumed to be linearly polarized along the different axes. The frequency is  $\omega = 0.1 \text{ eV}/\hbar$  and the field strength is taken to be  $E_0 = 0.5 \text{ V/\AA}$ . The relaxation rate is taken to be  $\hbar\gamma = 50 \text{ meV}$ . It is also shown the molecular excitonic lines (lower curves, except the line near  $0.5 \text{ eV}$ ). The latter is obtained at the excitation of  $C_{60}$  and  $C_{70}$  with probe laser pulse of frequency  $0.5 \text{ eV}/\hbar$  and  $E_0 = 10^{-4} \text{ V/\AA}$ . The relaxation rate is taken to be  $\hbar\gamma = 0.5 \text{ meV}$ . The spectra are shown for moderate EEI energy:  $U = 2 \text{ eV}$ .

EEI Hamiltonian with on-site and inter-site Coulomb repulsion energies  $U$  and  $V_{ij}$ , respectively. Since the distance  $d_{ij}$  between the nearest-neighbour pairs varies over the system, we scale inter-site Coulomb repulsion:  $V_{ij} = V d_{\min}/d_{ij}$ , where  $d_{\min}$  is the minimal nearest-neighbor distance. For the all calculations we use the ratio  $V = 0.4U$  [52, 54]. In the Hamiltonian, we neglected the lattice vibrations. In the calculations, the light-matter interaction is described in the length-gauge via the pure scalar potential

$$\hat{H}_{\text{int}} = e \sum_{i\sigma} \mathbf{r}_i \cdot \mathbf{E}(t) c_{i\sigma}^\dagger c_{i\sigma}, \quad (3)$$

with the elementary charge  $e$ , position vector  $\mathbf{r}_i$ , and the electric field strength  $\mathbf{E}(t) = f(t) E_0 \hat{\mathbf{e}} \cos \omega t$ , with the frequency  $\omega$ , polarization  $\hat{\mathbf{e}}$  unit vector, and pulse envelope  $f(t) = \sin^2(\pi t/\mathcal{T})$ . The pulse duration  $\mathcal{T}$  is taken to be 20 wave cycles:  $\mathcal{T} = 40\pi/\omega$ . From the Heisenberg equation one can obtain evolutionary equations for the single-particle density matrix  $\rho_{ij}^{(\sigma)} = \langle c_{j\sigma}^\dagger c_{i\sigma} \rangle$ . In addition, we will assume that the system relaxes at a rate  $\gamma$  to the equilibrium  $\rho_{0ij}^{(\sigma)}$  distribution. To obtain a closed set of equations for the single-particle density matrix  $\rho_{ij}^{(\sigma)} = \langle c_{j\sigma}^\dagger c_{i\sigma} \rangle$ , EEI will be considered under the Hartree-Fock approximation [58]. Thus, we obtain the following equation for the density matrix:

$$i\hbar \frac{\partial \rho_{ij}^{(\sigma)}}{\partial t} = \sum_k \left( \tau_{kj\sigma} \rho_{ik}^{(\sigma)} - \tau_{ik\sigma} \rho_{kj}^{(\sigma)} \right) + (V_{i\sigma} - V_{j\sigma}) \rho_{ij}^{(\sigma)} + e\mathbf{E}(t) (\mathbf{r}_i - \mathbf{r}_j) \rho_{ij}^{(\sigma)} - i\hbar\gamma (\rho_{ij}^{(\sigma)} - \rho_{0ij}^{(\sigma)}), \quad (4)$$

where  $V_{i\sigma} = \sum_{j\alpha} V_{ij} (\rho_{jj}^{(\alpha)} - \rho_{0jj}^{(\alpha)}) + U (\rho_{ii}^{(\sigma)} - \rho_{0ii}^{(\sigma)})$  and  $\tau_{ij\sigma} = t_{ij} + V_{ij} (\rho_{ji}^{(\sigma)} - \rho_{0ji}^{(\sigma)})$  are defined via the density matrix  $\rho_{ij}^{(\sigma)}$  and its initial value.

We numerically diagonalize the tight-binding Hamiltonian  $\hat{H}_0$  with the parameters that provide molecular orbitals close to experiment [56–58], and construct the initial density matrix  $\rho_{0ij}^{(\sigma)}$  via the filling of electron states in the valence band according to the zero temperature Fermi–Dirac-distribution  $\rho_{0ij}^{(\sigma)} = \sum_{\mu=N/2}^{N-1} \psi_\mu^*(j) \psi_\mu(i)$ , where  $\psi_\mu(i)$  is the eigenstate of  $\hat{H}_0$ .

**Results**– The HHG spectrum is evaluated from the Fourier transformation  $\mathbf{a}(\Omega)$  of the dipole acceleration  $\mathbf{a}(t) = d^2 \mathbf{d}/dt^2$ . The dipole is defined as  $\mathbf{d}(t) = e \sum_{i\sigma} \mathbf{r}_i \rho_{ii}^{(\sigma)}(t)$ . For convenience, we normalize the dipole acceleration by the factor  $a_0 = e\bar{\omega}^2 \bar{d}$ , where  $\bar{\omega} = 1 \text{ eV}/\hbar$  and  $\bar{d} = 1 \text{ \AA}$ . The power radiated at the given frequency is proportional to  $|\mathbf{a}(\Omega)|^2$ .

In order to clarify main aspects of HHG in  $C_{60}$  and  $C_{70}$ , we assume the excitation frequency is much smaller than the typical gap  $\sim 2 \text{ eV}$ . For all calculations the wave is assumed to be linearly polarized. Orienting the linearly polarized pump wave along different axes results in different harmonics spectra. The difference is essential for  $C_{70}$ . This is because for  $C_{70}$  the inversion symmetry takes place only for the 5-fold rotation axes (z-axis). In Fig. 1(a-f), we show the HHG spectra in the strong field regime ( $E_0 = 0.5 \text{ V/\AA}$ ) for different orientation of the wave’s polarization. For  $C_{60}$  molecule, because of the inversion symmetry only the odd harmonics appear in the HHG spectrum. For  $C_{70}$  molecule we have both even and odd harmonics except at the z-polarization of the pump wave. The

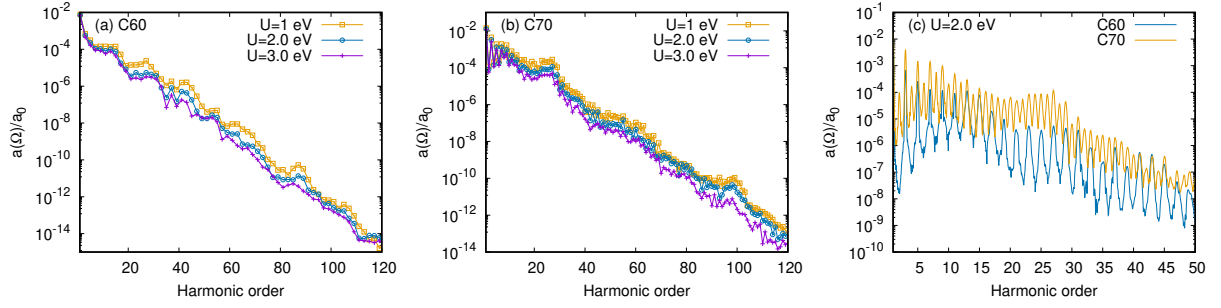


FIG. 2: The envelopes of HHG spectra (only peaks are connected) in the strong-field regime for different EEI energies in logarithmic scale via the normalized dipole acceleration Fourier transformation  $a(\Omega)/a_0$  (in arbitrary units) for  $C_{60}$  (a) and  $C_{70}$  (b). The frequency is  $\omega = 0.1 \text{ eV}/\hbar$  and the field strength is taken to be  $E_0 = 0.5 \text{ V/\AA}$ . The relaxation rate is taken to be  $\hbar\gamma = 50 \text{ meV}$ . In (c) we show HHG for  $C_{60}$  versus  $C_{70}$ .

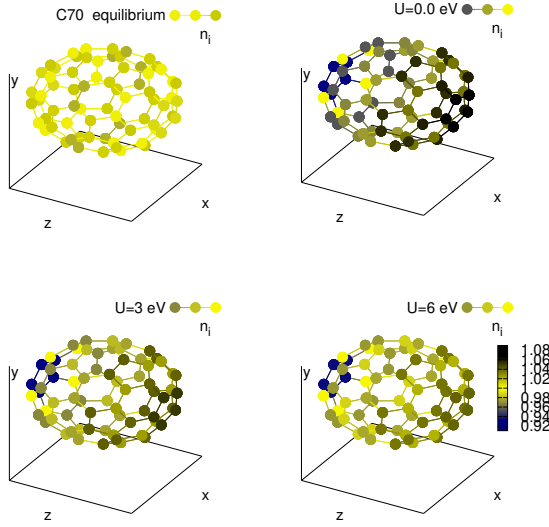


FIG. 3: The site occupations  $n_i$  in 3D color mapped molecular structures for  $C_{70}$ . The wave is assumed to be linearly polarized along the  $z$ -axis. The first configuration is the equilibrium, the next 3 configurations are at the peak of the laser field  $t = T/2$  for different EEI energies.

insets in Figs. 1(a) and 1(d) show low harmonics, where the difference in symmetry for  $C_{60}$  and  $C_{70}$  is clearly visible (see, also [58] for a relatively weak field). As is seen from Fig. 1, in both cases HHG spectra have a multi plateau structure that is connected with the intrinsic molecular excitations between the occupied molecular orbitals and the unoccupied molecular orbital. To show this in a more transparent way, in Fig. 1 it is also shown the molecular excitonic lines. The latter is obtained at the excitation of  $C_{60}$  and  $C_{70}$  with probe weak laser pulse. In particular, the lines near  $2.7 \text{ eV}$  and  $1.7 \text{ eV}$  for  $C_{60}$  and  $C_{70}$ , respectively, are the first dipole-allowed transition from highest occupied molecular orbital to the lowest unoccupied molecular orbital. These excitonic lines were termed as noninteger harmonics in [48] have their fingerprints in the multi plateau structure for the HHG spectra in the strong-field regime. As

is seen, plateaus' borders are defined by these lines. Besides for  $C_{70}$  there are close lines which enhance the HHG yield compared with  $C_{60}$ .

Since the boundaries of the plateaus are determined by dipole-allowed multiple electronic transitions between the molecular orbitals, it can be argued that for the frequencies  $\hbar\omega \ll t_{ij}$  these boundaries are almost invariant with respect to the pump wave frequency. They are determined through the intrinsic features of the free fullerene. Note also that the position of excitonic lines and relative intensities depend also on EEI. Besides, as was shown in [59], the on-site EEI suppresses the charge fluctuation and reduces the absorbed energy. It is also expected HHG yield suppression due to EEI. The latter is shown in Fig. 2, where the HHG spectra in the strong-field regime for different EEI energies are shown. To obtain the mean picture which does not depend on the orientation of the molecule with respect to laser polarization we take the wave polarization unit vector as  $\hat{\mathbf{e}} = 1/\sqrt{3}\{1, 1, 1\}$ . To make the plateaus more visible in Figs. 2(a) and 2(b) we show the envelopes of HHG spectra. As is seen from Figs. 2(a) and 2(b), with the increase of the EEI energy overall the HHG rate is suppressed. Another interesting aspect of HHG in fullerene is the qualitative and quantitative difference between both molecules. As is seen, the  $C_{70}$  molecule shows more pronounced nonlinear properties (Fig. 2(c)). Due to broken inversion symmetry in the case of  $C_{70}$ , we have even harmonics, besides due to the smaller energy gap and the larger density of states the HHG rate is larger by one to two orders compared with  $C_{60}$ . For comparison, in Fig. 2(c) we show the first four plateaus for both molecules. The suppression of HHG with the increase of EEI energy is connected with the fact that at strong on-site and inter-site electron-electron repulsion the polarizability of molecules or in other words electrons migration from the equilibrium states is suppressed. To show this visually, in Fig. 3 we display site occupations  $n_i = \langle c_{i\uparrow}^\dagger c_{i\uparrow} \rangle + \langle c_{i\downarrow}^\dagger c_{i\downarrow} \rangle$  via 3D color mapped molecular structures at the peak of the laser field for  $z$ -polarized wave for the same interaction parameters. The color bar represents site occupation. As can be seen from Fig. 3, the deviation from the equilibrium position and, therefore, the polarization is maximum for vanishing EEI.

We also investigated the HHG spectra dependence versus

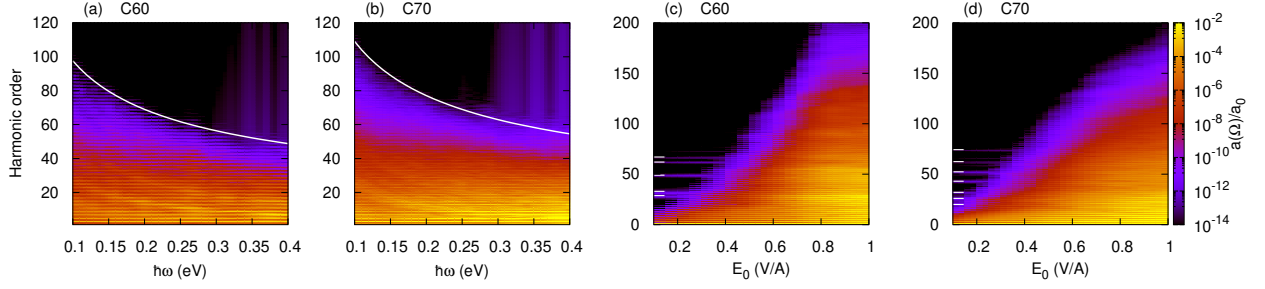


FIG. 4: The HHG spectra versus pump wave frequency (a,b) and intensity (c,d). The color bar represents the emission rate via dipole acceleration Fourier transformation  $a(\Omega)/a_0$  in the logarithmic scale for  $C_{60}$  (a, c) and  $C_{70}$  (b,d). The wave is assumed to be linearly polarized with polarization unit vector  $\hat{e} = \frac{1}{\sqrt{3}}\{1, 1, 1\}$ . The field strength is fixed  $E_0 = 0.5$  V/Å for (a) and (b), while for (c) and (d) the frequency is fixed  $\omega = 0.1$  eV/ħ. The spectra are shown for moderate EEI energy:  $U = 2$  eV. The relaxation rate is taken to be  $\hbar\gamma = 50$  meV. The white lines in (a) and (b) are envelopes  $\alpha/\sqrt{\omega}$  which show the cutoff harmonic positions. The white horizontal lines in (c) and (d) are excitonic resonances that show each plateau's borders.

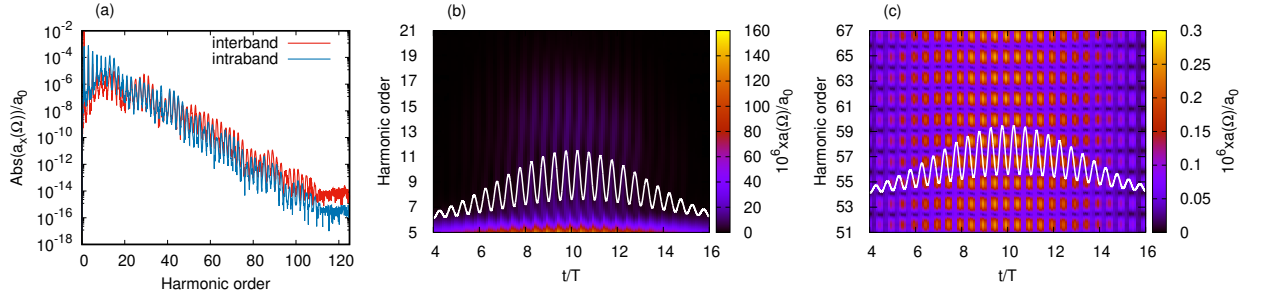


FIG. 5: The interband and intraband contribution in HHG spectra (a) and the spectrogram (b,c) of the HHG process via the windowed Fourier transform of the dipole acceleration for  $C_{60}$ . The wave is assumed to be linearly polarized with polarization unit vector  $\hat{e} = \frac{1}{\sqrt{3}}\{1, 1, 1\}$ . The frequency is  $\omega = 0.1$  eV/ħ and the field strength is taken to be  $E_0 = 0.5$  V/Å. The spectra are shown for  $U = 2$  eV and  $\hbar\gamma = 50$  meV. (b) low frequency part and (c) high frequency part. Then, the white curve on the density plots is scaled by the factor 10 population of the initially unoccupied molecular orbitals versus time.

pump wave frequency and intensity. In Figs. 4(a) and 4(b) we plot the HHG spectra versus pump wave frequency at moderate EEI energy  $U = 2$  eV, for  $C_{60}$  and  $C_{70}$ , respectively. For both molecules, the cutoff harmonic position is well approximated by the dependence  $N_{\text{cut}} \sim \omega^{-1/2}$  which is plotted along with density plot. Note that for atomic HHG via free continuum  $N_{\text{cut}} \sim \omega^{-3}$  [6]. In case of two-level atom  $N_{\text{cut}} \sim \omega^{-1}$  [60]. Thus, in contrast to atomic cases for fullerene molecule with the increase of the pump wave photon energy the cutoff harmonic energy ( $\hbar\omega N_{\text{cut}}$ ) is increased.

Next, we consider the HHG spectra as a function of pump wave intensity. In Figs. 4(c) and 4(d), we show the HHG spectra as a function of field amplitude and the harmonic order for a fixed frequency. The HHG spectra have interesting structures. First of all, it is clearly seen excitonic lines (marked by the white horizontal lines). These excitonic lines define the borders of the plateaus and within each plateau, the cutoff harmonic linearly increases with increasing the field strength. Then, reaching the harmonic  $\sim 160$  which corresponds to the transition of the lowest occupied molecular orbital to the highest unoccupied molecular orbital, the HHG rate is saturated.

Note that linear dependence of the cutoff harmonics on the field strength is inherent to HHG via discrete levels [60], or in crystals with linear energy dispersion [22, 23, 37].

We now consider the origin of the HHG in fullerene molecules. There are two contributions to the current: the electron/hole transitions within unoccupied/occupied molecular orbitals and the electron-hole creation (transitions from occupied molecular orbitals to unoccupied ones) and subsequent recombination. The former makes contribution only for low harmonics and is analogous to the intraband current in a semiconductor, while the latter makes the main contribution in the high frequency part corresponds to the interband current, which represents recombination/creation of electron-hole pairs. This picture is analogous to HHG in solid state systems. To separate these contributions in the dipole acceleration spectrum we made change of the basis via formula  $\rho_{ij} = \sum_{\mu'} \sum_{\mu} \psi_{\mu'}^*(j) \rho_{\mu\mu'} \psi_{\mu}(i)$ , where  $\rho_{\mu\mu'}$  is the density matrix in the energetic representation. Hence, we define interband

part of dipole acceleration, as

$$\mathbf{d}_{\text{inter}}(t) = 2 \sum_{\mu'=N/2}^{N-1} \sum_{\mu=0}^{N/2-1} \text{Re}(\rho_{\mu\mu'}(t) \mathbf{d}_{\mu'\mu}), \quad (5)$$

and intraband part will be

$$\mathbf{d}_{\text{intra}}(t) = \sum_{\mu,\mu'=N/2}^{N-1} \rho_{\mu\mu'}(t) \mathbf{d}_{\mu'\mu} + \sum_{\mu,\mu=0}^{N/2-1} \rho_{\mu\mu'}(t) \mathbf{d}_{\mu'\mu}, \quad (6)$$

where dipole transition matrix elements are  $\mathbf{d}_{\mu'\mu} = e \sum_i \psi_{\mu'}^*(i) \mathbf{r}_i \psi_{\mu}(i)$ . In Fig. 5(a), we show the inter-band/intraband contribution in HHG spectra for C<sub>60</sub>. The similar picture we have for C<sub>70</sub>. As is seen, intraband dipole acceleration is significant for low frequency part of the spectrum, while in the high frequency part the main contribution is caused by the electron-hole creation and subsequent recombination. This information can also be extracted from the evolution of the high harmonic spectrum as a function of time. For this propose a Blackman window of width  $1.2\pi/\omega$  is scanned across 20 optical cycles. The results along with the population of the conduction band (unoccupied molecular orbitals)  $W(t) = \sum_{\mu=0}^{N/2-1} \rho_{\mu\mu}(t)$  are displayed in Figs. 5(b) and 5(c). As is seen from these figures, the emission of high harmonics takes place two times per wave cycle, corresponding to two maxima or minima of the population. The low frequency harmonic bursts take place in-between maxima and minima of the population Fig. 5(b), while higher harmonics are the results of the recombination and the bursts take place at minima of the population (Fig. 5(c)). There are also a domain of harmonics where we have interplay between intra- and interband emission.

**Conclusion**— We revealed the general features of the HHG in fullerene molecule under strong-field driving. The HHG spectra show multiple plateaus, which is explained by the recombination of electrons and holes from molecular orbitals. Those are intrinsic molecular excitations between the unoccupied molecular orbitals and the occupied molecular orbital. These intrinsic molecular excitations – so-called excitonic lines define the borders of the plateaus. Within the each plateau, the cutoff harmonic linearly increases with increasing the field strength. In contrast to atomic cases, for fullerene molecule with the increase of the pump wave photon energy the cutoff harmonic energy is increased. The HHG spectra strongly depends on the molecule symmetry qualitatively as well as quantitatively. The C<sub>70</sub> molecule shows more pronounced non-linear properties due to degradation of molecular symmetry compared with C<sub>60</sub>. We also revealed the role of EEI. With the increase of the EEI energy overall the HHG rate is suppressed. The fullerene molecules are known to have different isomers with other point-group symmetries. Therefore, they are interesting systems as a new sources of HHG, and spectroscopy based on HHG might be useful to reveal the symmetries and electron dynamics involved. Developing a detailed understanding of the HHG in different classes of fullerene molecule is an interesting topic for the future work.

This work was supported by the RA State Committee of Science in the frame of the research project 20TTWS-1C010.

\* Electronic address: mkrтчian@ysu.am

- [1] H. K. Avetissian, *Relativistic Nonlinear Electrodynamics: The QED Vacuum and Matter in Super-Strong Radiation Fields* (Springer, Berlin 2015).
- [2] A. Di. Piazza, C. Müller, K. Z. Hatsagortsyan, and C. H. Keitel, *Rev. Mod. Phys.* **84**, 1177 (2012).
- [3] P. Agostini, L. F. DiMauro, *Rep. Prog. Phys.* **67** 813 (2004).
- [4] M. C. Kohler, T. Pfeifer, K. Z. Hatsagortsyan, and C. H. Keitel, *Adv. Atom. Mol. Opt. Phys.* **61**, 159 (2012).
- [5] P. B. Corkum, *Phys. Rev. Lett.* **71**, 1994 (1993).
- [6] M. Lewenstein, P. Balcou, M. Y. Ivanov, A. L'Huillier, and P. B. Corkum, *Phys. Rev. A* **49**, 2117 (1994).
- [7] P. B. Corkum and F. Krausz, *Nat. Phys.* **3**, 381 (2007).
- [8] F. Krausz and M. Ivanov, *Rev. Mod. Phys.* **81**, 163 (2009).
- [9] H. Lakhota, H. Y. Kim, M. Zhan, S. Hu, S. Meng, and E. Goulielmakis, *Nature* **583**, 55 (2020).
- [10] R. E. F. Silva, I. V. Blinov, A. N. Rubtsov, O. Smirnova, and M. Ivanov, *Nature Photon.* **12**, 266 (2018).
- [11] D. Bauer and K. K. Hansen, *Phys. Rev. Lett.* **120**, 177401 (2018).
- [12] G. Vampa, T. J. Hammond, N. Thiré, B. E. Schmidt, F. Légaré, C. R. McDonald, T. Brabec, D. D. Klug, and P. B. Corkum, *Phys. Rev. Lett.* **115**, 193603 (2015).
- [13] N. Tancogne-Dejean, O. D. Mücke, F. X. Kartner, and A. Rubio, *Phys. Rev. Lett.* **118**, 087403 (2017).
- [14] C. G. Wahlström, J. Larsson, A. Persson, T. Starczewski, S. Svanberg, P. Salieres, P. Balcou, and A. L'Huillier, *Phys. Rev. A* **48**, 4709 (1993).
- [15] T. D. Donnelly, T. Ditmire, K. Neuman, M. D. Perry, and R. W. Falcone, *Phys. Rev. Lett.* **76**, 2472 (1996).
- [16] C. Vozzi, M. Nisoli, J. Caumes, G. Sansone, S. Stagira, S. De Silvestri, M. Vecchiocattivi, D. Bassi, M. Pascolini, L. Poletto, P. Villorresi, and G. Tondello, *Appl. Phys. Lett.* **86**, 111121 (2005).
- [17] O. Smirnova, Y. Mairesse, S. Patchkovskii, N. Dudovich, D. Villeneuve, P. Corkum, and M. Yu. Ivanov, *Nature* **460**, 972 (2009).
- [18] S. Ghimire, A. D. DiChiara, E. Sistrunk, P. Agostini, L. F. DiMauro, and D. A. Reis, *Nature Phys.* **7**, 138 (2011).
- [19] B. Zaks, R. B. Liu, and M. S. Sherwin, *Nature* **483**, 580 (2012).
- [20] F. Langer, M. Hohenleutner, C. P. Schmid, C. Poellmann, P. Nagler, T. Korn, C. Schüller, M. S. Sherwin, U. Huttner, J. T. Steiner, S. W. Koch, M. Kira, R. Huber, *Nature* **533**, 225 (2016).
- [21] O. Schubert, M. Hohenleutner, F. Langer, B. Urbanek, C. Lange, U. Huttner, D. Golde, T. Meier, M. Kira, S. W. Koch, and R. Huber, *Nature Photon.* **8**, 119 (2014).
- [22] G. Vampa, C. R. McDonald, G. Orlando, D. D. Klug, P. B. Corkum, and T. Brabec, *Phys. Rev. Lett.* **113**, 073901 (2014).
- [23] G. Vampa, C. R. McDonald, G. Orlando, P. B. Corkum, and T. Brabec, *Phys. Rev. B* **91**, 064302 (2015).
- [24] G. Ndashimiye, S. Ghimire, M. Wu, D. A. Browne, K. J. Schafer, M. B. Gaarde, and D. A. Reis, *Nature* **534**, 520523 (2016).
- [25] Y. S. You, D. A. Reis, and S. Ghimire, *Nature Phys.* **13**, 345349 (2017).
- [26] H. Liu, C. Guo, G. Vampa, J. L. Zhang, T. Sarmiento, M. Xiao, P. H. Bucksbaum, J. Vuckovic, S. Fan, and D. A. Reis, *Nature Phys.* **14**, 1006 (2018).
- [27] S. A. Mikhailov and K. Ziegler, *J. Phys. Condens. Matter* **20**,

- 384204 (2008).
- [28] H. K. Avetissian, A. K. Avetissian, G. F. Mkrtchian, and K. V. Sedrakian, *Phys. Rev. B* **85**, 115443 (2012).
  - [29] H. K. Avetissian, G. F. Mkrtchian, K. G. Batrakov, S. A. Maksimenko, and A. Hoffmann, *Phys. Rev. B* **88**, 165411 (2013).
  - [30] P. Bowlan, E. Martinez-Moreno, K. Reimann, T. Elsaesser, and M. Woerner, *Phys. Rev. B* **89**, 041408(R) (2014).
  - [31] I. Al-Naib, J. E. Sipe, and M. M. Dignam, *Phys. Rev. B* **90**, 245423 (2014).
  - [32] H. K. Avetissian and G. F. Mkrtchian, *Phys. Rev. B* **94**, 045419 (2016).
  - [33] L. A. Chizhova, F. Libisch, and J. Burgdorfer, *Phys. Rev. B* **95**, 085436 (2017).
  - [34] D. Dimitrovski, L. B. Madsen, and T. G. Pedersen, *Phys. Rev. B* **95**, 035405 (2017).
  - [35] N. Yoshikawa, T. Tamaya, and K. Tanaka, *Science* **356**, 736 (2017).
  - [36] H. K. Avetissian and G. F. Mkrtchian, *Phys. Rev. B* **97**, 115454 (2018).
  - [37] H. K. Avetissian, A. K. Avetissian, B. R. Avchyan, G. F. Mkrtchian, *Phys. Rev. B* **100**, 035434 (2019).
  - [38] H. K. Avetissian and G. F. Mkrtchian, *Phys. Rev. B* **99**, 085432 (2019).
  - [39] H. Liu, Y. Li, Y. S. You, S. Ghimire, T. F. Heinz, and D. A. Reis, *Nat. Phys.* **13**, 262 (2017).
  - [40] H. K. Avetissian, G. F. Mkrtchian, and K. Z. Hatsagortsyan, *Phys. Rev. Research* **2**, 023072 (2020).
  - [41] G. Le Breton, A. Rubio, and N. Tancogne-Dejean, *Phys. Rev. B* **98**, 165308 (2018).
  - [42] H. W. Kroto, J. R. Heath, S. C. O'Brien, R. F. Curl, and R. E. Smalley, *Nature* **318**, 162 (1985).
  - [43] W. Krätschmer, L. Lamb, K. Fostiropoulos, and D. R. Huffman, *Nature* **347**, 354 (1990).
  - [44] S. Iijima, *Nature* **354**, 56 (1991).
  - [45] A. K. Geim, I. V. Grigorieva, *Nature* **499**, 419 (2013).
  - [46] R. A. Ganeev, L. B. Elouga Bom, J. Abdul-Hadi, M. C. H. Wong, J. P. Brichta, V. R. Bhardwaj, and T. Ozaki, *Phys. Rev. Lett.* **102**, 013903 (2009).
  - [47] R. A. Ganeev, L. B. Elouga Bom, M. C. H. Wong, J.-P. Brichta, V. R. Bhardwaj, P. V. Redkin, and T. Ozaki, *Phys. Rev. A* **80**, 043808 (2009).
  - [48] G. P. Zhang, *Phys. Rev. Lett.* **95**, 047401 (2005).
  - [49] G. P. Zhang and T. F. George, *Phys. Rev. A* **74**, 023811 (2006).
  - [50] G. P. Zhang and T. F. George, *J. Optical Society of America B* **24**, 1150 (2007).
  - [51] G. P. Zhang and Y. H. Bai, *Phys. Rev. B* **101**, 081412(R) (2020).
  - [52] R. L. Martin, J. P. Ritchie, *Phys. Rev. B* **48**, 4845 (1993).
  - [53] G. P. Zhang, *Phys. Rev. B* **56**, 9189 (1997).
  - [54] G. P. Zhang, *Phys. Rev. B* **61**, 4377 (2000).
  - [55] G. Chiappe, E. Louis, E. San-Fabian, and J. A. Verges, *J. Phys.: Condens. Matter* **27**, 463001 (2015).
  - [56] R. W. Lof, M. A. Van Veenendaal, B. Koopmans, H. T. Jonkman, G. A. Sawatzky, *Phys. Rev. Lett.* **68**, 3924 (1992).
  - [57] T. Rabenau, A. Simon, R. K. Kremer, and E. Sohmen, *Z. Phys. B* **90**, 69 (1993).
  - [58] See Supplemental Materials for details of the theoretical model.
  - [59] G. P. Zhang, *Phys. Rev. Lett.* **91**, 176801 (2003).
  - [60] H. K. Avetissian, B. R. Avchyan, G. F. Mkrtchian, *J. Phys. B* **45**, 025402 (2012).